Formation of kinetically trapped small clusters of PEGylated gold nanoparticles revealed by the combination of small-angle X-ray scattering and visible light spectroscopy

Daniel Szekrényes, Cyrille Hamon, Doru Constantin, András Deák

▶ **To cite this version:**

Daniel Szekrényes, Cyrille Hamon, Doru Constantin, András Deák. Formation of kinetically trapped small clusters of PEGylated gold nanoparticles revealed by the combination of small-angle X-ray scattering and visible light spectroscopy. Soft Matter, 2022, 18 (43), pp.8295-8301. 10.1039/D2SM01257J . hal-03838184

HAL Id: hal-03838184
https://hal.science/hal-03838184

Submitted on 3 Nov 2022

HAL is a multi-disciplinary open access archive for the deposit and dissemination of scientific research documents, whether they are published or not. The documents may come from teaching and research institutions in France or abroad, or from public or private research centers.

L'archive ouverte pluridisciplinaire **HAL**, est destinée au dépôt et à la diffusion de documents scientifiques de niveau recherche, publiés ou non, émanant des établissements d'enseignement et de recherche français ou étrangers, des laboratoires publics ou privés.

Distributed under a Creative Commons Attribution - NonCommercial 4.0 International License

Formation of Kinetically Trapped Small Clusters of PEGylated Gold Nanoparticles Revealed by the Combination of Small-angle X-ray Scattering and Visible Light Spectroscopy

Daniel P. Szekrényes,[a] Cyrille Hamon,[b] Doru Constantin,[b,c*] András Deák[a*]

Gold nanoparticles coated with polyethylene glycol (PEG) are able to form clusters due to the collapse of the surface-grafted polymer chains when the temperature and ion concentration of the aqueous medium are increased. The chain collapse reduces the steric repulsion, leading to particle aggregation. In this work, we combine small angle X-ray scattering (SAXS) and visible light spectroscopy to elucidate the structure of the developing clusters. The structure derived from the SAXS measurements reveals a decrease in interparticle distance and drastic narrowing of its distribution in the cluster, indicating restricted particle mobility and displacement within the cluster. Surprisingly, instead of forming a large crystalline phase, the evolving clusters are composed of about a dozen particles. The experimental optical extinction spectra measured during cluster formation can be very well reproduced by optical simulations based on the SAXS-derived structural data.

Introduction

The interest in the localized plasmon resonance supported by metallic nanoparticles fostered intensive research not only related to the fundamental aspects of nanoparticle plasmons, but also regarding possible applications that derive from the plasmonic properties.[1] Near-field effects and plasmon coupling upon particle aggregation are of special interest, as these are widely used in simple particle aggregation and plasmonic hot-spot based analyte detection schemes.[2] The attractivity of the simple, ensemble-based optoplasmonic sensing approach lies in its simplicity compared to more advanced techniques, which can undoubtedly provide more detailed information, but require a rather complex infrastructure.[3] It has to be emphasized, however, that the underlying particle aggregation or clustering requires the (partial) loss of colloidal stability and the resulting cluster structure will depend on the strength of the attractive colloidal interactions.[4,5] One straightforward way to tune the aggregation is by controlled reduction of solvent quality in surface-grafted polymer-stabilized nanoparticle systems.[6,7] On the other hand, depending on the structure of the cluster and on the distance between the particles within the clusters, the resulting optical spectrum can have markedly different characteristics. When only a few particles participate in forming the clusters and/or their structure is well defined, the resulting optical changes can be well interpreted with the help of optical calculations.[8–10] For larger and 3D aggregates, or when the structure is less defined, the interpretation of the spectra is difficult due to the usually broad peak emerging in the NIR region of the spectrum as a result of a multitude of overlapping optically dominant coupled plasmon modes.[11,12]

We have shown earlier, that the bulk phase clustering of PEG covered gold nanoparticles can be triggered by raising the temperature at elevated background ion concentration, leading to the formation of large and compact nanoparticle clusters with ordered internal structure.[5] The driving force of the process is the developing soft-sphere type colloidal pair interaction energy profile as a result of surface grafted polymer chain collapse,[13] and has been shown theoretically to be critical in the preparation of ordered nanoparticle clusters.[14] Kinetic control of the clustering process can be also realized by controlling the concentration and temperature levels, leading to particle aggregates with different sizes.[15] Our concept has been confirmed by others, preparing 2D and 3D aggregates of PEGylated gold nanoparticles, indicating a hexagonal (FCC) arrangement of the particles in the nanoparticle solid.[4,16–18] It is important to note, that this clustering approach differs substantially from creating *ab ovo* unstable systems or aggregation schemes relying on (macro)molecular linkers,[8,19] but belongs to the broader family of solvent quality tuning based aggregation approaches.[6,7,20]

In this work, we aimed to investigate the development of nanoparticle clusters, where the driving force for clustering is rather moderate, favoring the formation of smaller particle aggregates. We investigated the assembly of PEGylated nanoparticles by a combined SAXS and visible light spectroscopy approach in order to consistently link these independent measurement results to the structural changes. The measurements were interpreted by theoretical calculations both of the structure factor and of the extinction spectra. We showed that SAXS provides a detailed picture of the cluster structure and can capture subtle structural changes as a function of temperature. By full-curve fitting the measured SAXS data, we found compact clusters composed of only a moderate number of particles, instead of the formation a large crystalline nanoparticle solid phase. Optical extinction measurements to follow the clustering process of gold nanoparticles are far easier to perform, but they are less sensitive to fine details of the cluster structure as aggregation-related plasmon coupling dominates the observed spectral changes. Realistic agreement between simulated and measured optical spectra can be obtained, however, if the SAXS derived structural data is used as input for the simulations and the surface damping of the localized nanoparticle surface plasmons is also taken into account. Besides demonstrating the

advantages in combining SAXS and spectroscopy approaches for the study of particle clustering, the results also underline that special care is required when only simple ensemble optical measurements are employed to monitor the clustering of gold nanoparticles - an approach that is broadly applied in various detection schemes.

Experimental

For nanoparticle synthesis, surface modification and clustering hydrogen tetrachloroaurate trihydrate (99,9%), sodium citrate tribasic dihydrate (99%), potassium sulfate (99%) were obtained from Sigma-Aldrich and thiolated polyethylene glycol (mPEG-SH, 750 Da) was purchased from Rapp Polymere GmbH. All chemicals were used as received. For all experiments, ultrapure water with a resistivity of 18.2 MΩcm was used. The glassware was cleaned using aqua regia.

The spherical nanoparticles were prepared by the traditional Turkevich method,[21] while their PEGylation was carried out as reported earlier.[5] Visible light extinction spectroscopy was realized using a fiber coupled stabilized tungsten halogen light source (Thorlabs SL201L) and spectrometer (Thorlabs CCS200) at different temperatures in a cuvette holder (Thorlabs CVH100) with laboratory built external temperature control. Three different temperature values (35°C, 45°C and 55°C) and two different potassium sulfate concentrations (0.125M and 0.25M) were considered. The gold concentration is always 7.2 nM, corresponding to a volume fraction $\varphi_P = 10^{-5}$.

For recording the optical extinction spectra, a custom written Labview software was used. Before recording the spectra, the temperature of both the nanoparticle sol and the salt solution was set to the desired value and the dilution of the salt solution upon injection was taken into account. The temperature was kept constant during the measurement. Optical simulations of the nanoparticles' and nanoparticle clusters' extinction spectra were performed by the MNPBEM MATLAB module,[22] using the dielectric function of gold given by Olmon et al.[23] This dielectric function was modified to include an interfacial damping term, which accounts for surface scattering of the conduction electrons and for chemical interface damping.[24] The simulation algorithm accounts for retardation and the effective refractive index of the embedding medium was set to 1.467 due to the presence of PEG. The particles and the particle assemblies were illuminated along the *x*, *y* and *z* principal axes each with two perpendicular polarizations and the extinction spectrum was obtained by averaging over these 6 excitations. Ten different, randomized nanoparticle cluster structures were simulated and averaged in each case, generated in the same way as for the SAXS evaluation (see Supplementary Information).

SAXS experiments were carried out using the SWING beamline at SOLEIL synchrotron facility, at an energy of 16 keV. The sample-detector distance was set to 6.223 m. The scattered intensity as a function of q vector modulus was obtained by radially averaging the measured scattering pattern using the FOXTROT software developed at the beamline. This SAXS signal ($I(q)$) can be written in the form of $I(q)=nV^2\Delta\rho^2P(q)S(q)$, where V is the volume of the particle and $\Delta\rho$ is the difference in scattering length density between the particle and the surrounding medium. The form factor, denoted by $P(q)$, normalized such that $P(q\rightarrow0) = 1$, is due to the size and the shape of the particles, while the structure factor $S(q)$ provides information on their configuration. To determine the experimental structure factor, the SAXS signal of assembled nanospheres was divided by a polydisperse sphere model fit to the initial (well-dispersed) sample: $I_0(q)\ S(q) = I(q)/I_{model}(q)$. As shown in the ESI, $I_{model}(q)$ *is very close to* $I_0(q)$, confirming that interparticle interactions can be neglected at room temperature. Note also that, due to this polydispersity, $S(q)$ is strictly speaking an effective structure factor and is only equal to the true structure factor in the decoupling approximation: $\langle V^2P(q)S(q)\rangle = \langle V^2P(q)\rangle\langle S(q)\rangle$: considering the low relative polydispersity (about 10%), we neglect this effect in the following.

Results and discussion

The SAXS measurements of the as-prepared particle sample yielded a core diameter of 14.2 ± 1.3 nm (mean ± SD, see Supplementary Information Figure S1). Combined with the gold concentration, this parameter yields a number concentration of particles $n_P = 6.5\ 10^{-9}\ \mathrm{nm}^{-3}$. The prepared samples are kinetically stable, as in addition to the electric double layer repulsion the end-grafted polymer chains also counteracts the van der Waal attraction. When the PEGylated particles are placed in a salt solution, however, their aggregation can be induced at elevated temperature due to the collapse of the surface-grafted polymer chains and the decrease of the associated steric repulsion between particles (Scheme 1).[5,18] Depending on the resulting colloidal interaction profile, destabilization can lead either to relatively slow nanoparticle cluster formation, or to rapid aggregation,[25] similar to the results obtained on 'hairy' and plain silica nanoparticles.[26]

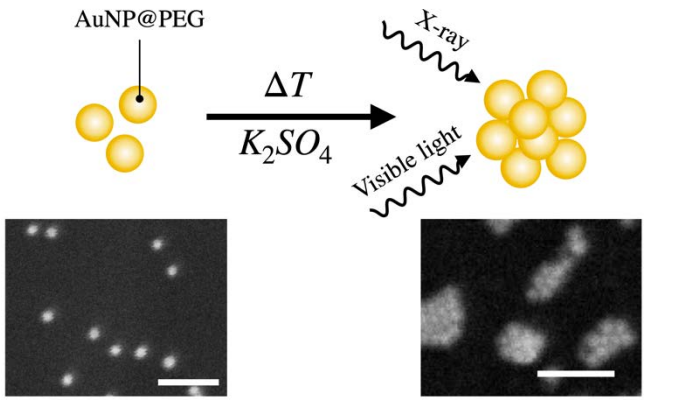

Scheme 1. PEGylated gold nanoparticles can form nanoparticle clusters when the temperature and ion concentration in the system is increased. The clustering leads to a pronounced change of the small-angle X-ray scattering and visible light extinction spectra. Scale bars: 100 nm.

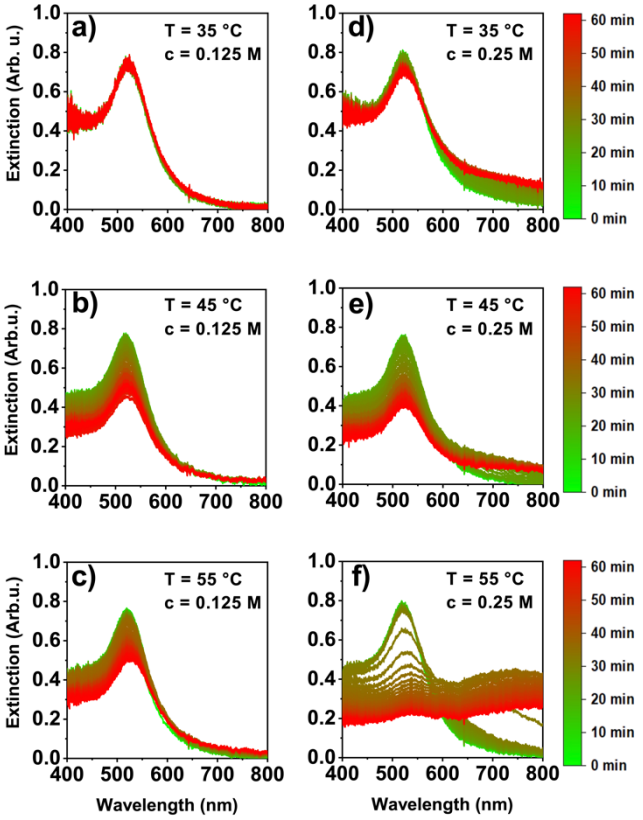

Figure 1. Time evolution of the ensemble optical extinction spectra recorded at different ion concentrations and temperatures after addition of the salt solution. The extinction peak around 520 nm corresponding to the dipolar localized plasmon resonance redshifts upon clustering (a-e), while additional extreme broadening due to a multitude of coupled modes is observed upon rapid aggregation (f)

When a soft-sphere type interaction curve is present due to a strong short range repulsion (due to PEG in the present case) with only a small (few *kT*) attractive potential minimum, the particles will assemble into fairly ordered colloidal clusters.[14] Larger attractive potentials on the other hand results in fast aggregation rates and the diffusion limited growth produces fractal-like aggregates.[27,5]

For the PEGylated particles used in the present study, the decreasing stability of the particles with increasing temperature can be clearly detected in their time-dependent visible extinction spectra (Figure 1).At the lowest investigated salt concentration and temperature (0.125 M; 35 °C) the sample remains stable and no change in the extinction maximum nor in the width of the peak can be observed. As the temperature is increased to 45 or 55 °C, however, a small redshift is observed and the extinction measured in the visible wavelength range decreases continuously. As the extinction value around 400 nm is dominated by interband transition instead of the localized plasmon resonance, its value correlates with the amount of Au^0 in the light path.[28] Hence, this observed decrease already indicates that some particles leave the detection volume, that is, the samples sediment to some extent. The effect of sedimentation can be separated from the changes induced by plasmon coupling by performing a renormalization of the extinction spectra at 400 nm. The renormalized spectra (for details see Supplementary Information Figure S2) at 0.125 M for the 45 and 55 °C case show a small redshift and (especially for the 55 °C case) peak broadening can be observed, with slightly increasing extinction in the near infrared region. This plasmon-coupling-related effect confirms that the nanoparticles approach each other. On the other hand, the extent of the near-field coupling is small, indicating a rather large coordination distance. More pronounced spectral changes can be observed at higher, 0.25 M salt concentration. There is already a clear indication of cluster formation at 35 °C and the NIR extinction becomes dominant at higher temperature. At 55 °C a qualitatively different behavior is observed, with the appearance of a broad extinction peak in the NIR wavelength

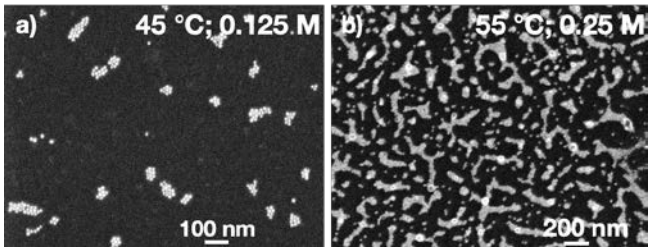

Figure 2: Scanning electron microscopy images of drop-casted samples taken after 60 minutes clustering time at 45 °C and 0.125 M (a) and 55 °C 0.25 M (b).

region, typical for the case of aggregation due to stronger interparticle attraction.[5,11] It appears that, even though clustering takes place at different concentration/temperature combinations, there is a fundamental difference in the extent of clustering and/or in the resulting structure for the 0.25 M; 55 °C case. This is also indicated by SEM images taken from drop-casted samples after 60 minutes, which show that smaller clusters are formed at lower temperatures and ion concentrations (Figure 2). Note, however, that the structure of dried-in SEM samples might differ from that of the as-formed cluster structure in the liquid phase. The spectroscopy measurements also indicate that after 60 minutes the clustering process comes to a hold, and no further aggregation related spectral shifts can be anticipated, except for sedimentation of large aggregates.

SAXS investigation of the same systems was carried out to obtain more direct information about the structure of the evolving nanoparticle clusters. A locally compact nanosphere arrangement was assumed when evaluating the SAXS data,[29] locally similar to the FCC structure of the extended nanoparticle aggregates obtained with large (6 kDa) PEG grafted nanoparticles.[16]

Cluster configurations are generated starting from a starting arrangement with equal interparticle distances, by adding along the three space directions random position fluctuations drawn from a Gaussian distribution with a given standard deviation. The structure factor of these objects is computed using the Debye equation. Our approach is similar to Hansen's Monte Carlo method.

The structure factor depends sensitively on the average separation distance between the particles, its distribution, the number of spheres in the cluster as well as on the fraction of free versus clustered nanoparticles (see Supplementary Information Figure S3 for details). It is noteworthy that the calculated structure factors show the average of 1000 individual

configurations, the corresponding particle-particle separation distribution functions are shown as insets in Figure 3. The main parameters obtained from the SAXS measurements are listed in Table 1; particle surface separation refers to gold particle surface-to-surface distance, α is the ratio of clustered to all particles. The time evolution of the SAXS measurements (Supplementary Figures S4 and S5.) corresponds to the spectral changes observed using visible light spectroscopy, that is, cluster formation proceeds rather slowly on the hour scale, and the clusters do not completely disintegrate when the system is cooled back to 25 °C.

Table 1 Structural parameters obtained from SAXS measurements at different salt concentrations and temperatures.

	Particle surface separation (Å)	Fraction of clustered particles - α
0.125 M; 45 °C	27.9 ± 13.3	0.63
0.125 M; 55 °C	27.5 ± 13.8	0.78
0.25 M; 45 °C	26.0 ± 12.4	0.83
0.25 M; 55 °C	18.0 ± 1.7	0.96

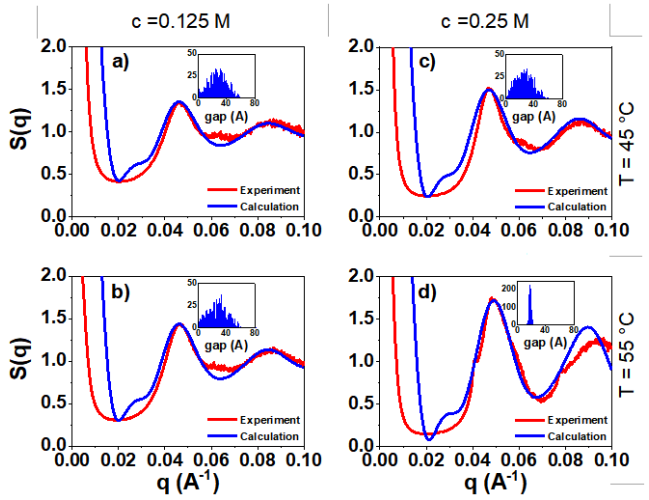

Figure 3. Measured and calculated structure factors for the nanoparticle clusters obtained at different ion concentration and temperature: a) 0.125 M, 45 °C; b) 0.125 M, 55 °C; c) 0.25 M, 45 °C; d) 0.25 M, 55 °C. The insets show the particle separation distribution (counts *vs.* gap size).

The structure factor calculations provide good agreement with the measurements in Figure 3.a)-c), whereas for the sample measured at 0.25 M and 55 °C there is a clear difference at the peak around q=0.09. The experimental spectrum exhibits additional features around q=0.04 and q=0.08, not captured by the calculation. They might originate from the presence of more complex cluster structures. It is important to emphasize that the best agreement with the experimental data was obtained assuming N=13 particles in the cluster, regardless of salt concentration and temperature (Supplementary Information Figures S6 and S7 for the demonstration). This also suggests that, in spite of the obvious nanoparticle association, the system is kinetically trapped in the few-particle cluster state, without developing huge particle aggregates. This conclusion is coherent with the results of the time-dependent spectroscopy measurements shown above. Even for the highest investigated salt concentration and temperature (0.25 M and 55 °C), the loose coordination of the smaller clusters can be anticipated, without leading to very large, compact aggregates. This is in agreement with the spectroscopic data (Figure 1) and the SEM images (Supplementary Information Figure S3).

The average gap between the particles in the clusters shows generally a decreasing trend as the ion concentration and the temperature increase. This is in qualitative agreement with recent results involving gold nanoparticles grafted with larger polymer chains.[17] More importantly, there is a fundamental difference in the particle separation distribution. While for a)-c) the gap between the particles covers a fairly broad range, in the case of d) there is a clear reduction of the particle separation and a pronounced narrowing of the gap distribution (also see Supplementary Information Figure S8). We attribute this difference to the collapse of the surface-grafted PEG chains, which results in a deeper potential well in terms of colloidal interactions due to reduction of the steric repulsion range,[5,15] and the attractive forces effectively lock the particles in place as the cluster is formed. This also explains the trend observed during the visible light extinction measurements: as long as the PEG only shrinks, the particles experience only moderate attraction and are separated from each other due to the still effective steric repulsion, so both the particle coordination within the cluster and the plasmon coupling will be rather weak. When PEG collapses, on the other hand, it leads to aggregation with small interparticle separations and hence to pronounced plasmon coupling. This conclusion is also supported by the calculated nanoparticle pair interaction potentials (Supplementary Information Figure S9). An initial PEG brush thickness of 1.85 nm can be inferred from dynamic light scattering experiments.[5] As a rough estimate, the SAXS-based surface separation values listed in Table 1 divided by a factor of 2 indicate ca. 25% smaller values (ca. 50% in the 0.25 M; 55 °C case); the separation data in Table 1 were used as input to obtain the steric interaction contribution. As expected, at these high ion concentrations the electric double layer interaction is basically absent with Debye lengths well below 1 nm (Supplementary Information Figure S9), the interaction is dominated by the balance of the attractive dispersion and repulsive steric interactions.[5] While there is a steady decrease of the interaction energy minimum, for the 0.25 M; 55 °C sample its depth drops well below -5 kT. This also means that while the particle separation is reduced, the strong interparticle attraction impedes reorganization of the particles within the clusters, enabling the growth of non-centrosymmetric clusters.[14] The observed trend of α is also in line with the derived structural data and the colloidal interaction calculations. It indicates that the fraction of nanoparticles incorporated in a cluster gradually increases with ion concentration and temperature.

To confirm this scenario, data derived from the SAXS measurements was used as input for optical simulations and the clusters' optical extinction spectra were compared with the experimental ones. As the particles used in this study are well below the mean free electron path length (ca. 37.7 nm for

gold),[30] the conduction electrons will scatter at the particle surface. Additionally, PEG is attached to the particles' surface via a thiol moiety, resulting in an additional chemical surface damping (CID) of the plasmons. For spherical particles, the combined effect of surface scattering and chemical interface damping can be given as the interfacial damping $\Gamma_{int} = Av_F/R$, where v_F is the Fermi velocity (1.4 nm/fs)[31] and R is the particle radius in nanometers . A is the combined surface and CID – or interfacial – parameter, which is of order unity and can be taken into account in simulations by modifying the bulk dielectric function of gold.[24] As shown in Figure 4.a, the increase of the interfacial damping contribution results in a blueshift and broadening of the individual particle's resonance. While in theory the size of the nanoparticles as well as the polydispersity can affect both the position and width of the dipole resonance,

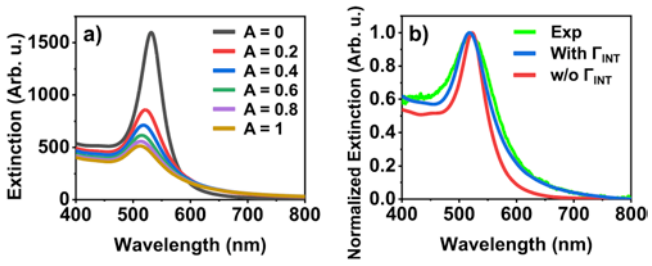

Figure 4. a) Simulated extinction spectra of 14.2 nm diameter gold nanospheres without (A=0) and with increasing interfacial damping contribution. b) Comparison of the experimental spectrum with the calculated ones without (A=0) and with interfacial damping term (A=0.35).

for the given particle size their influence is negligible (Supplementary Information Figure S10). As a consequence, the measured ensemble optical extinction spectrum can be compared to a particle's calculated spectrum. Following the approach of Berciaud et al.,[32] setting the interfacial (combined surface and CID) parameter to A=0.35 yields very good agreement with the experimental spectrum (Figure 4.b). Our A parameter is somewhat larger than the previously reported value (A = 0.25) for similarly sized gold nanospheres,[32] which is the result of chemical linkage between the gold surface and the thiolated PEG in the present case, leading to a larger CID contribution,[33] close to the value obtained for CTAB-capped gold nanoparticles ($A \approx 0.35$).[34,35]

The good agreement of the measured and calculated spectra allows the calculation of the nanoparticle clusters' spectra, with clusters constructed based on the SAXS-derived data. The cluster extinction spectrum simulation not only includes the separation distance and distribution values, but the fraction of particles incorporated in the clusters as well. This latter is done by dividing first the calculated cluster spectrum with the corresponding number of particles, yielding the average spectral contribution of a single clustered particle. The final simulated spectrum is then calculated as the sum of the spectral contributions from clustered and free particles with weighting factors α and 1-α for the clustered and free particles, respectively, where the value of α is taken from the corresponding SAXS evaluation (Table 1). The comparison of the starting and final (after 60 minutes) measurement with the optical calculations is shown in Figure 5. It is noteworthy that we achieve excellent agreement for a)-c), implying that the optical calculation based on the SAXS-derived structure effectively captures the small changes occurring during clustering.

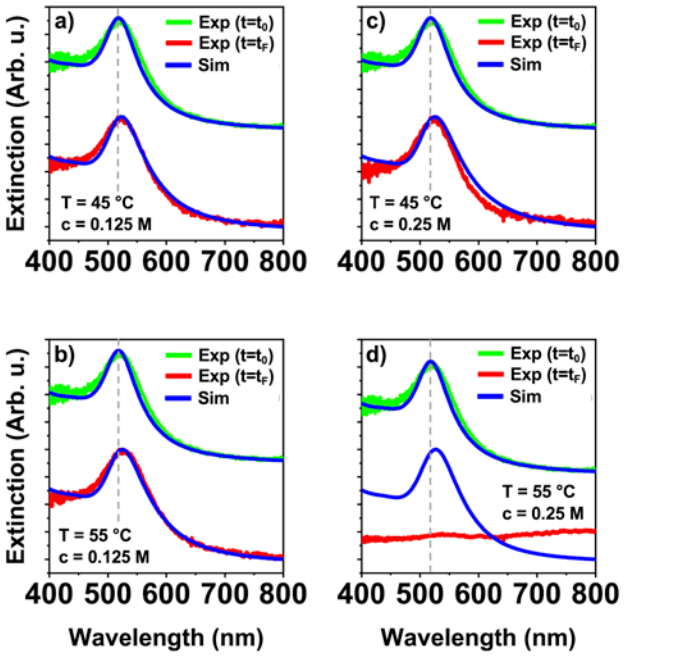

Figure 5. Experimental and simulated optical extinction spectra of the PEGylated gold nanosphere sols at different ion concentrations and temperatures at the beginning of the clustering process (t_0) and after 60 minutes (t_F) - spectra are vertically shifted for better visibility. The dashed vertical lines show the original position of the extinction maxima.

A similar spectral evolution for clustered gold nanoparticles was observed earlier for 3-mercatopropionate-induced clustering in the presence of PEG.[19] Note, however, that for the system indicating PEG collapse (0.25 M; 55 °C – Figure 5.d), the calculation fails to reproduce the experimental data: the emerging peak in the NIR wavelength region and the extreme broadening are not reproduced in the optical simulation. The measured spectrum for d) indicates that, as a result of strong interparticle attraction, elongated structures (e.g. chain-like aggregates) are also present, and extinction from these optically dominant modes determines the measured spectra.[4,11] Note that when the nanoparticle design limits the growth of the clusters (e.g. when Janus-type gold nanospheres are used where the clustering is self-limited due to anisotropic particle structure or encapsulation of the small clusters in a polymer shell), the optical spectrum does not show this extreme broadening.[9,36]

Conclusions

The combined small angle X-ray scattering and optical spectroscopy investigation of the clustering process for PEGylated gold nanospheres (ca. 14 nm; 750 Da PEG) indicated that it is possible to form ordered nanoparticle clusters that are composed of only a moderate number of particles. It was found that with increasing salt concentration and temperature the coordination of the nanospheres in the developing compact ordered clusters becomes stronger. It was found that before the

pronounced PEG chain collapse the coordinated particles are still separated by ca. 2.5-3 nm, meaning that steric repulsion between the polymer chains is still active. The optical measurements are consistent with the SAXS-derived data: although particle clustering takes place, the rapid aggregation cannot be observed, as indicated by only a redshift and broadening of the localized plasmon resonance peak. Optical simulation of the clusters corroborates these assumptions and leads to excellent agreement with the measured spectra. When the solvent conditions induce the collapse of the PEG chains, the average distance between the particles in the cluster strongly decreases. At the same time, the separation distance distribution is drastically narrowed, indicating a strong attraction and low mobility of the particles within the clusters. This is also reflected in the measured optical spectra, which – together with the optical simulations – indicate that more complex structures are also produced during clustering. Hence, when functionalized nanoparticles are employed as signal transducers (e.g. in plasmonic nanoparticle aggregation based sensing applications), cluster-structure related optical effects should be also considered carefully.

Acknowledgements

This work was supported by the French-Hungarian bilateral agreements Balaton Program - 41878TK and National Research, Development and Innovation Office – NKFIH, 2018-2.1.13-TÉT-FR-2018-00002 and NKFIH FK128327. We acknowledge SOLEIL for the provision of synchrotron radiation facilities, and thank Thomas Bizien for assistance in using beamline SWING.

Notes and references

1 L. Wang, M. Hasanzadeh Kafshgari and M. Meunier, *Adv. Funct. Mater.*, 2020, **30**, 2005400.
2 D. Vilela, M. C. González and A. Escarpa, *Analytica Chimica Acta*, 2012, **751**, 24–43.
3 J. Xavier, S. Vincent, F. Meder and F. Vollmer, *Nanophotonics*, 2018, **7**, 1–38.
4 N. K. Kwon, T. K. Lee, S. K. Kwak and S. Y. Kim, *ACS Appl. Mater. Interfaces*, 2017, **9**, 39688–39698.
5 D. Zámbó, G. Z. Radnóczi and A. Deák, *Langmuir*, 2015, **31**, 2662–2668.
6 R. M. Choueiri, A. Klinkova, H. Thérien-Aubin, M. Rubinstein and E. Kumacheva, *Journal of the American Chemical Society*, 2013, **135**, 10262–10265.
7 S. Izor, A. Schantz, A. Jawaid, C. Grabowski, T. Dagher, H. Koerner, K. Park and R. Vaia, *Macromolecules*, 2021, **54**, 10435–10446.
8 L. Guo, Y. Xu, A. R. Ferhan, G. Chen and D.-H. Kim, *J. Am. Chem. Soc.*, 2013, **135**, 12338–12345.
9 N. Castro, D. Constantin, P. Davidson and B. Abécassis, *Soft Matter*, 2016, **12**, 9666–9673.
10 J. Lyu, D. Alloyeau, C. Hamon and D. Constantin, *J. Mater. Chem. C*, 2021, **9**, 1730–1739.
11 R. W. Taylor, R. Esteban, S. Mahajan, R. Coulston, O. A. Scherman, J. Aizpurua and J. J. Baumberg, *The Journal of Physical Chemistry C*, 2012, **116**, 25044–25051.
12 D. Zámbó and A. Deák, *Periodica Polytechnica: Chemical Engineering*, 2016, **60**, 244–251.
13 N. Backmann, N. Kappeler, T. Braun, F. Huber, H.-P. Lang, C. Gerber and R. Y. H. Lim, *Beilstein Journal of Nanotechnology*, 2010, **1**, 3–13.
14 D. Klotsa and R. L. Jack, *Soft Matter*, 2011, **7**, 6294.
15 D. Zámbó, Sz. Pothorszky, D. F. Brougham and A. Deák, *RSC Adv.*, 2016, **6**, 27151–27157.
16 H. Zhang, W. Wang, M. Akinc, S. Mallapragada, A. Travesset and D. Vaknin, *Nanoscale*, 2017, **9**, 8710–8715.
17 H. J. Kim, W. Wang, S. Mallapragada, A. Travesset and D. Vaknin, *J. Phys. Chem. C*, 2021, **125**, 10090–10095.
18 H. J. Kim, W. Wang, H. Zhang, G. Freychet, B. M. Ocko, A. Travesset, S. K. Mallapragada and D. Vaknin, *Langmuir*, 2021, **37**, 10143–10149.
19 D. Van Haute, J. M. Longmate and J. M. Berlin, *Adv. Mater.*, 2015, **27**, 5158–5164.
20 H. Tao, E. Galati and E. Kumacheva, *Macromolecules*, 2018, **51**, 6021–6027.
21 J. Turkevich, P. C. Stevenson and J. Hillier, *Discuss. Faraday Soc.*, 1951, **11**, 55.
22 J. Waxenegger, A. Trügler and U. Hohenester, *Computer Physics Communications*, 2015, **193**, 138–150.
23 R. L. Olmon, B. Slovick, T. W. Johnson, D. Shelton, S.-H. Oh, G. D. Boreman and M. B. Raschke, *Physical Review B*, , DOI:10.1103/PhysRevB.86.235147.
24 H. Hövel, S. Fritz, A. Hilger, U. Kreibig and M. Vollmer, *Phys. Rev. B*, 1993, **48**, 18178–18188.
25 T. Gisler and M. Borkovec, *Langmuir*, 1993, **9**, 2247–2249.
26 M. Kobayashi, F. Juillerat, P. Galletto, P. Bowen and M. Borkovec, *Langmuir*, 2005, **21**, 5761–5769.
27 S. H. Behrens, D. I. Christl, R. Emmerzael, P. Schurtenberger and M. Borkovec, *Langmuir*, 2000, **16**, 2566–2575.
28 W. Haiss, N. T. K. Thanh, J. Aveyard and D. G. Fernig, *Analytical Chemistry*, 2007, **79**, 4215–4221.
29 A. Burke, M. Chevreuil, A. Paris, V. de La Grange, C. Goldmann, J. Pérez, D. Constantin and G. Tresset, *Phys. Rev. Applied*, 2018, **10**, 054065.
30 D. Gall, *Journal of Applied Physics*, 2016, **119**, 085101.
31 G. V. Hartland, *Chemical Reviews*, 2011, **111**, 3858–3887.
32 S. Berciaud, L. Cognet, P. Tamarat and B. Lounis, *Nano Lett.*, 2005, **5**, 515–518.
33 B. Foerster, A. Joplin, K. Kaefer, S. Celiksoy, S. Link and C. Sönnichsen, *ACS Nano*, 2017, **11**, 2886–2893.
34 C. Novo, D. Gomez, J. Perez-Juste, Z. Zhang, H. Petrova, M. Reismann, P. Mulvaney and G. V. Hartland, *Physical Chemistry Chemical Physics*, 2006, **8**, 3540.
35 K. Slyusarenko, B. Abécassis, P. Davidson and D. Constantin, *Nanoscale*, 2014, **6**, 13527–13534.
36 A. S. Urban, X. Shen, Y. Wang, N. Large, H. Wang, M. W. Knight, P. Nordlander, H. Chen and N. J. Halas, *Nano Letters*, 2013, **13**, 4399–4403.

Electronic Supplementary Information (ESI)

Formation of Kinetically Trapped Small Clusters of PEGylated Gold Nanoparticles Revealed by the Combination of Small-angle X-ray Scattering and Visible Light Spectroscopy

Daniel P. Szekrényes,[1] Cyrille Hamon,[2] Doru Constantin,[2,3*] András Deák[1]*

[1] Centre for Energy Research, Budapest, Hungary

[2] Université Paris-Saclay, CNRS, Laboratoire de Physique des Solides, 91405 Orsay, France

[3] Institut Charles Sadron, CNRS and Université de Strasbourg, 67034 Strasbourg, France

Corresponding Author

*Doru Constantin: constantin@unistra.fr

*András Deák: andras.deak@ek-cer.hu

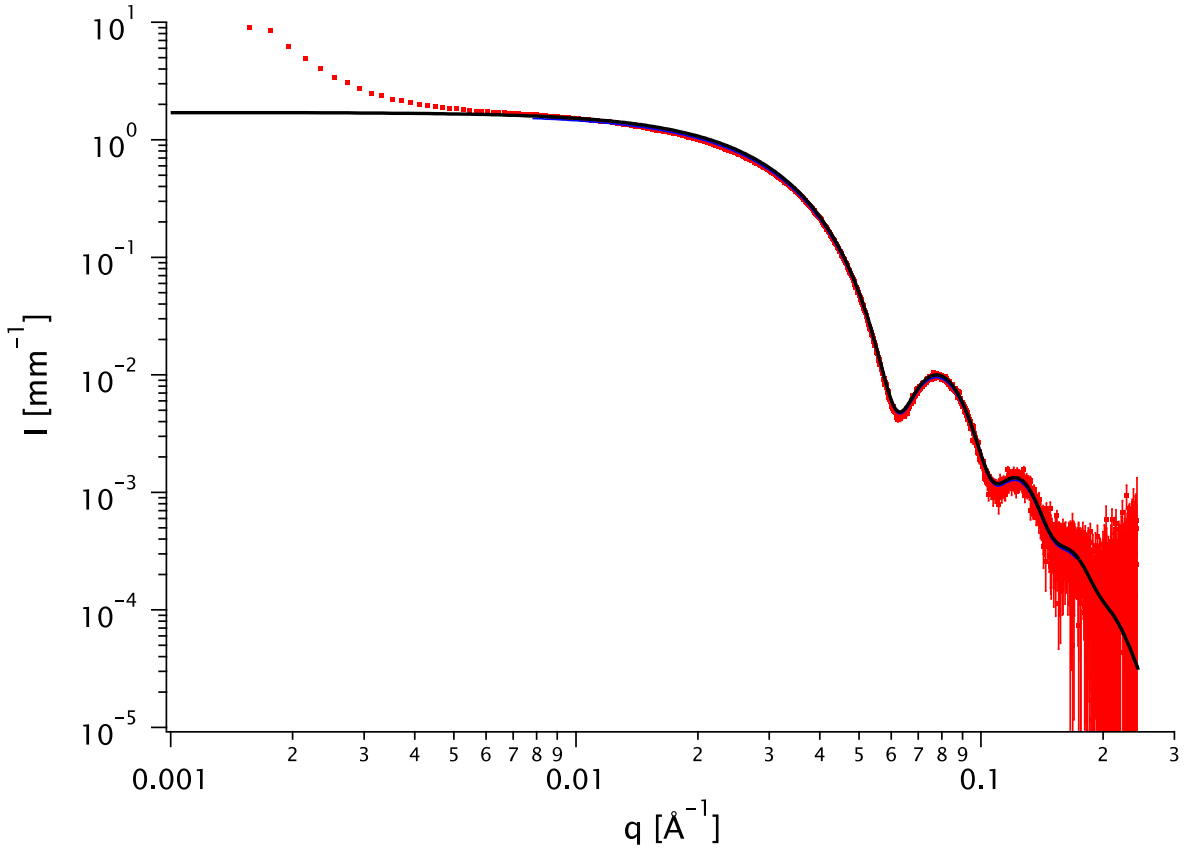

Figure S1: *SAXS signal of PEGylated gold nanospheres well dispersed in water (symbols) and fit with a polydisperse sphere model (solid line).*

The intensity scattered by the gold nanoparticles in dilute aqueous solution was fitted with a polydisperse sphere model (the polydispersity was described by a Schulz distribution). The mean diameter is $\langle 2a \rangle = 14.2$ nm and the standard deviation $\sigma = 1.3$ nm. The number concentration of the particles is $n_P = 6.5\ 10^{-9}$ nm^{-3}, corresponding to a volume fraction $\varphi_P = 10^{-5}$. In the

model we also use the appropriate scattering length density for gold and water at 16 keV: 108.2 and 9.44 $Å^{-2}$, respectively.

Renormalization of the extinction spectra

For aggregating plasmonic nanoparticle systems, the time evolution of the extinction spectrum change might contain both the effect of plasmon coupling (in the form of red-shift and eventual appearance of new extinction modes) and sedimentation (extinction decrease). As the extinction measured at 400 nm is depending only on the concentration of Au^0 in the light path, renormalizing the spectra at this wavelength can help to separate these two effects. Two examples are shown below. **Figure S2**a and b contain the raw extinction spectra. The extracted values at 400 nm are shown in **Figure S2**c and d. Due to the fluctuation, these time-dependent values are fitted with a linear curve; the parameters of which can be used to renormalize the extinction spectra at any arbitrary time. The result of the renormalization procedure is shown in **Figure S2**e-f, showing the impact of clustering on the extinction spectra.

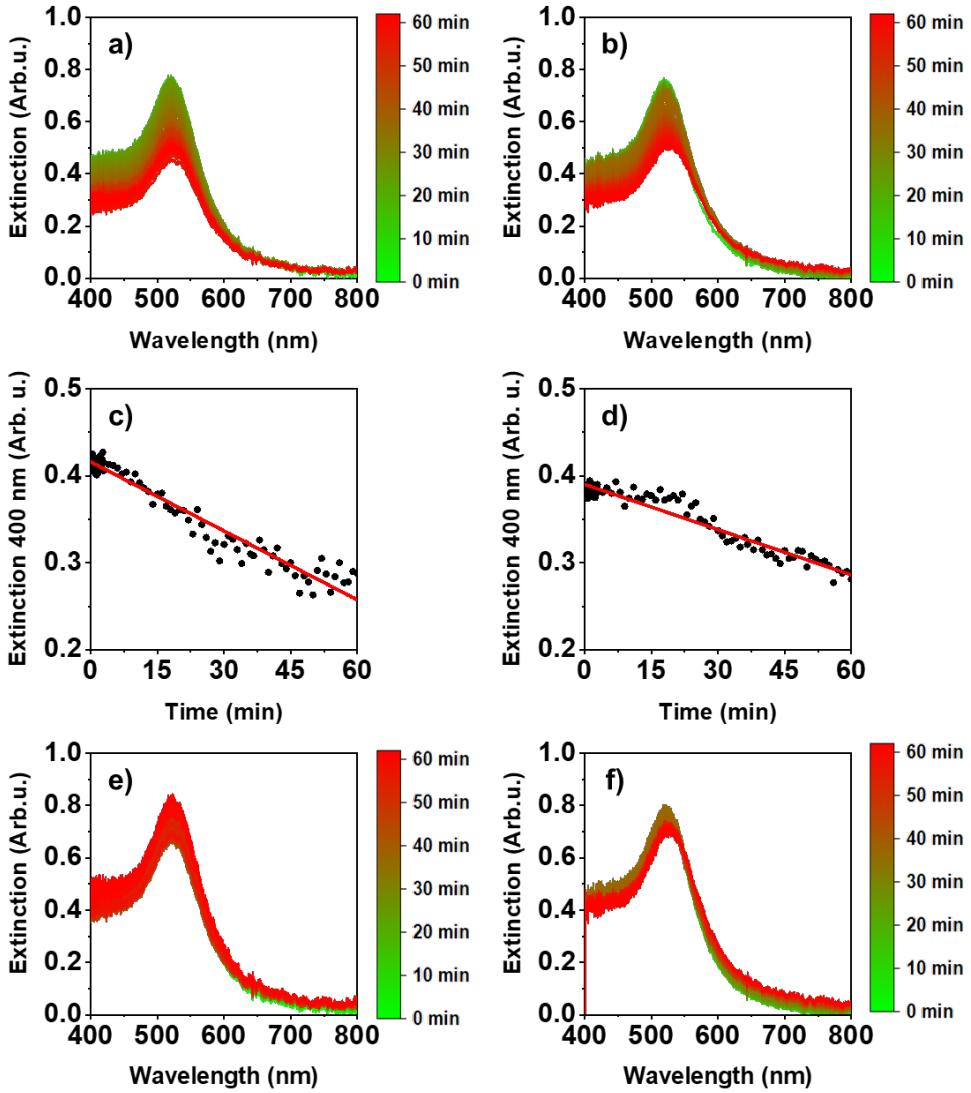

***Figure S2**: Time evolution of the ensemble extinction spectra when the ion concentration is 0.125 M, at 45 °C (a) and 55 °C (b). Decrease in extinction at 400 nm as a function of the elapsed time*

for 0.125 M, 45 °C (c) and 0.125 M, 55 °C (d). The linear fits are used for renormalization to obtain the corrected spectra e) 0.125 M, 45 °C and f) 0.125 M, 55 °C.

Simulation of the SAXS structure factor - S(q)

The simulated structure factor of the given arrangement of identical spherical scatterers was calculated according to the Debye scattering formula:

$$S(q) = 1 + \frac{2}{N}\sum_{i=1}^{N-1}\sum_{j=i+1}^{N}\frac{\sin(qr_{ij})}{qr_{ij}}$$

Based on the comparison of the calculated structure factor to the experimental one, the configuration of the particle clusters was systematically changed to obtain a best fit of the measurement result. Assuming isotropic interactions around the nanoparticles, a cluster containing 13 particles with compact arrangement was used; 12 particles surround a center particle. During the simulation the distance between the neighboring particles was adjusted. The particles can fluctuate around this equilibrium position along the x, y and z direction based on Gaussian distribution, resulting in different gaps (surface-to-surface distance) between the gold nanospheres; the standard deviation of this distribution is set as input parameter. The clustering rate is also accounted for by linearly combining the structure factor of the given clusters (renormalized with the number of particles in the cluster) with the structure factor of free particles S(q)=1. The weighting factor for the linear combination are α and (1- α) for the clustered and the free particles, respectively, that is α represents; the ratio of clustered to all particles in the system (e.g. at α=0.4 40% of the particles are incorporated in a cluster)

The number of particles in a cluster is an additional parameter used for tuning the structure factor to achieve the best fit. In a typical simulation 1000 measurements were performed and their average was compared to the experimental structure factor. **Figure S3** summarizes the effect of different input parameters on the calculated structure factor.

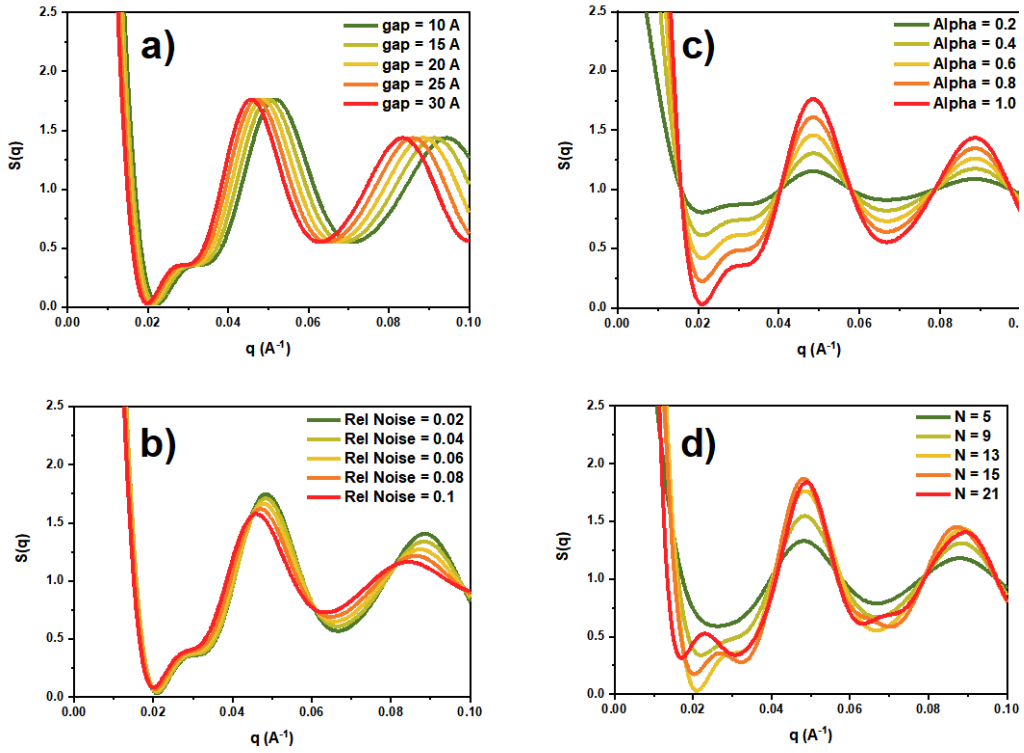

***Figure S3**: The effect of tuning a) interparticle distance, b) relative Gaussian noise, c) fraction of clustered particles and d) the number of particles on the calculated SAXS structure factor.*

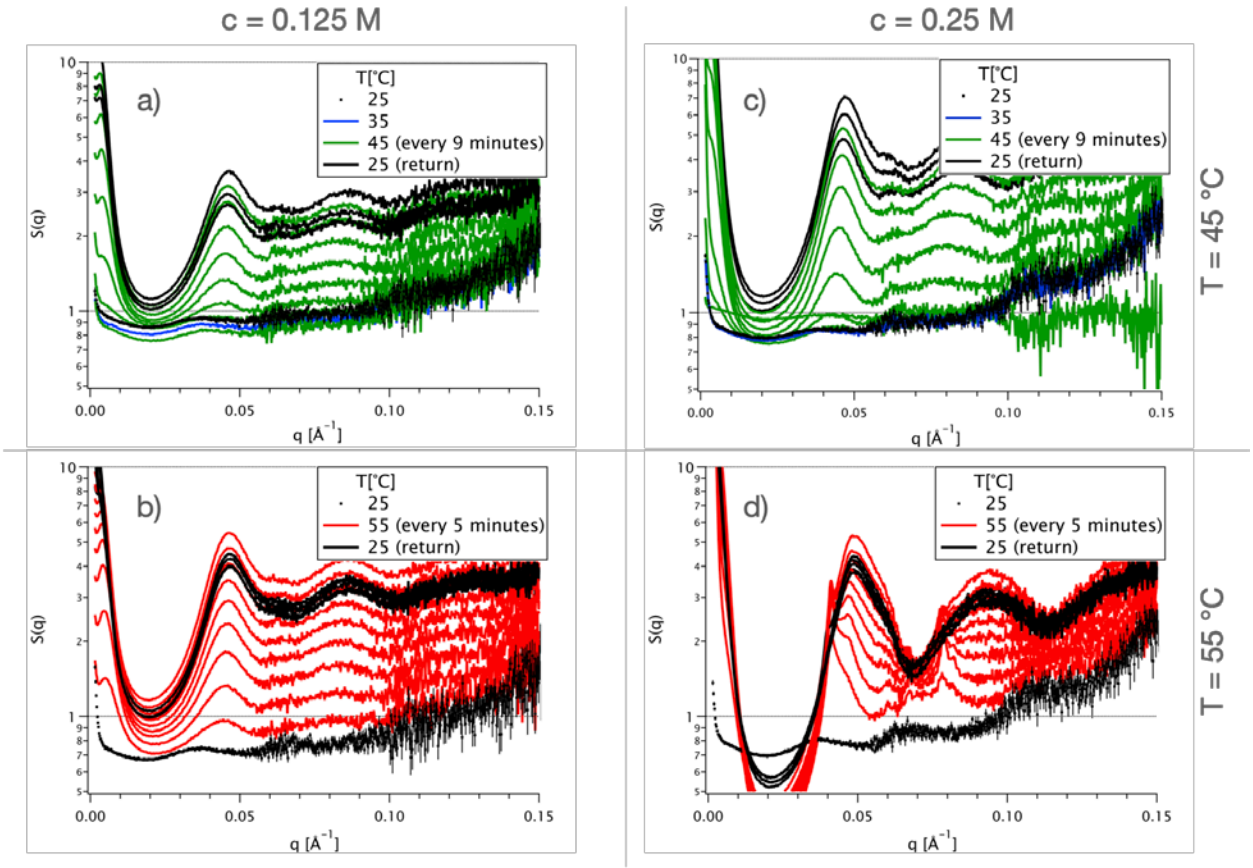

***Figure S4**: Time evolution of the structure factor obtained at different salt concentrations and temperatures. After clustering the system was returned to the initial temperature of 25 °C. The curves are shifted vertically for clarity.*

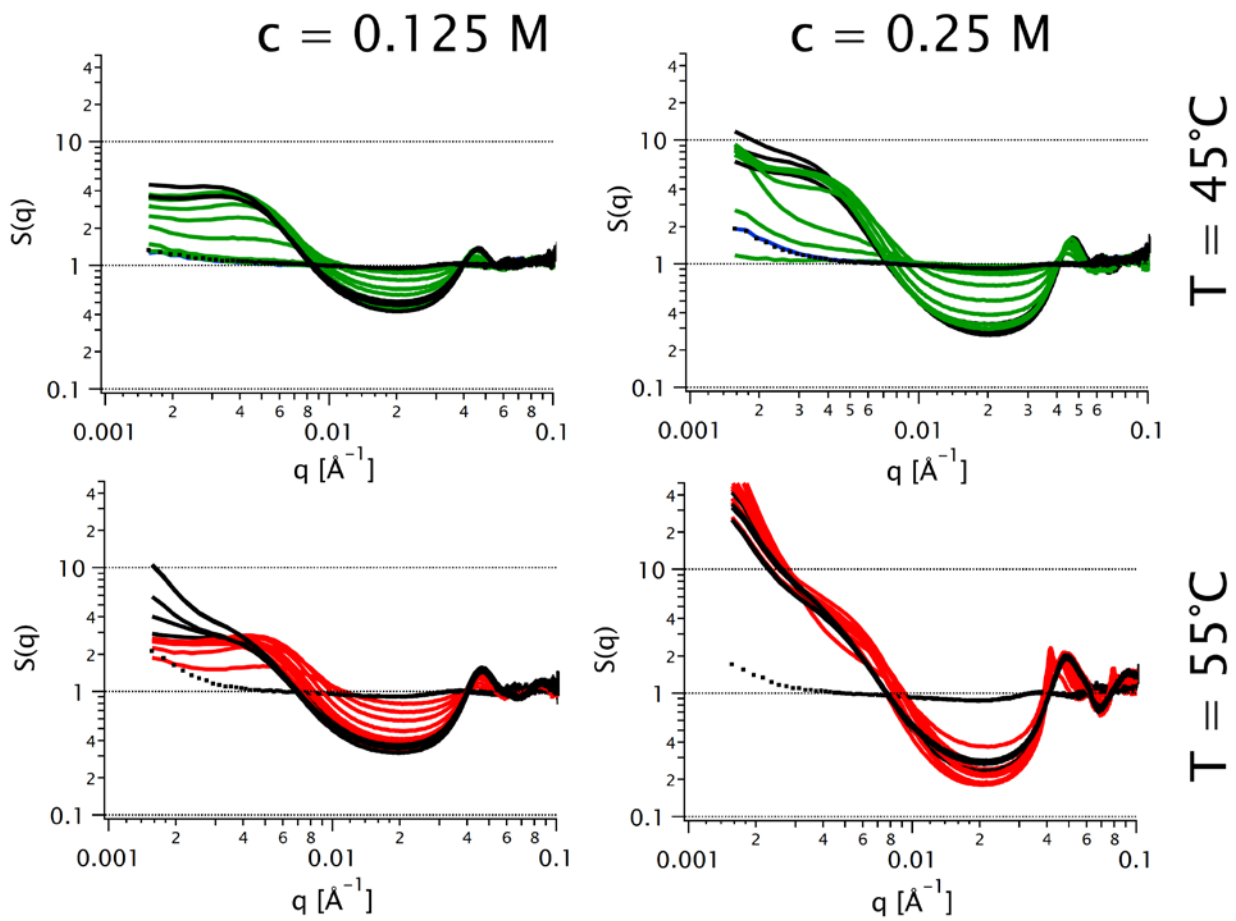

***Figure S5**: Same data as in **Figure S4**, but in log-log representation and without vertical shift.*

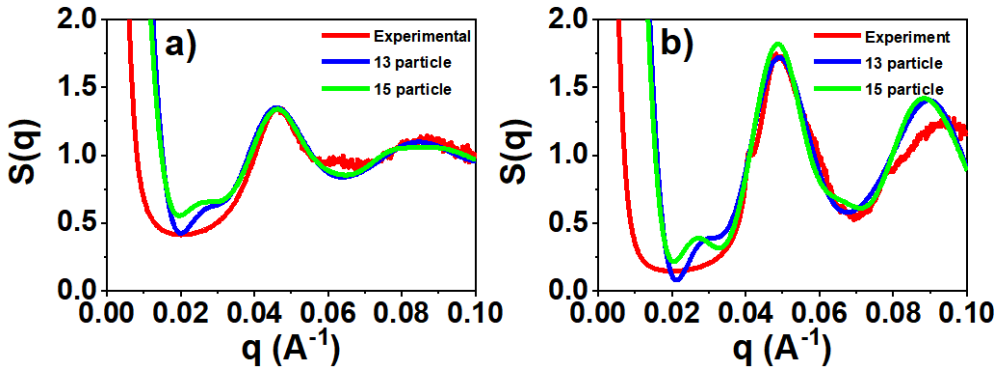

***Figure S6**: Experimental and calculated structure factors assuming 13 or 15 particles in the clusters for 0.125 M; 45 °C (a) and 0.25 M; 55 °C (b).*

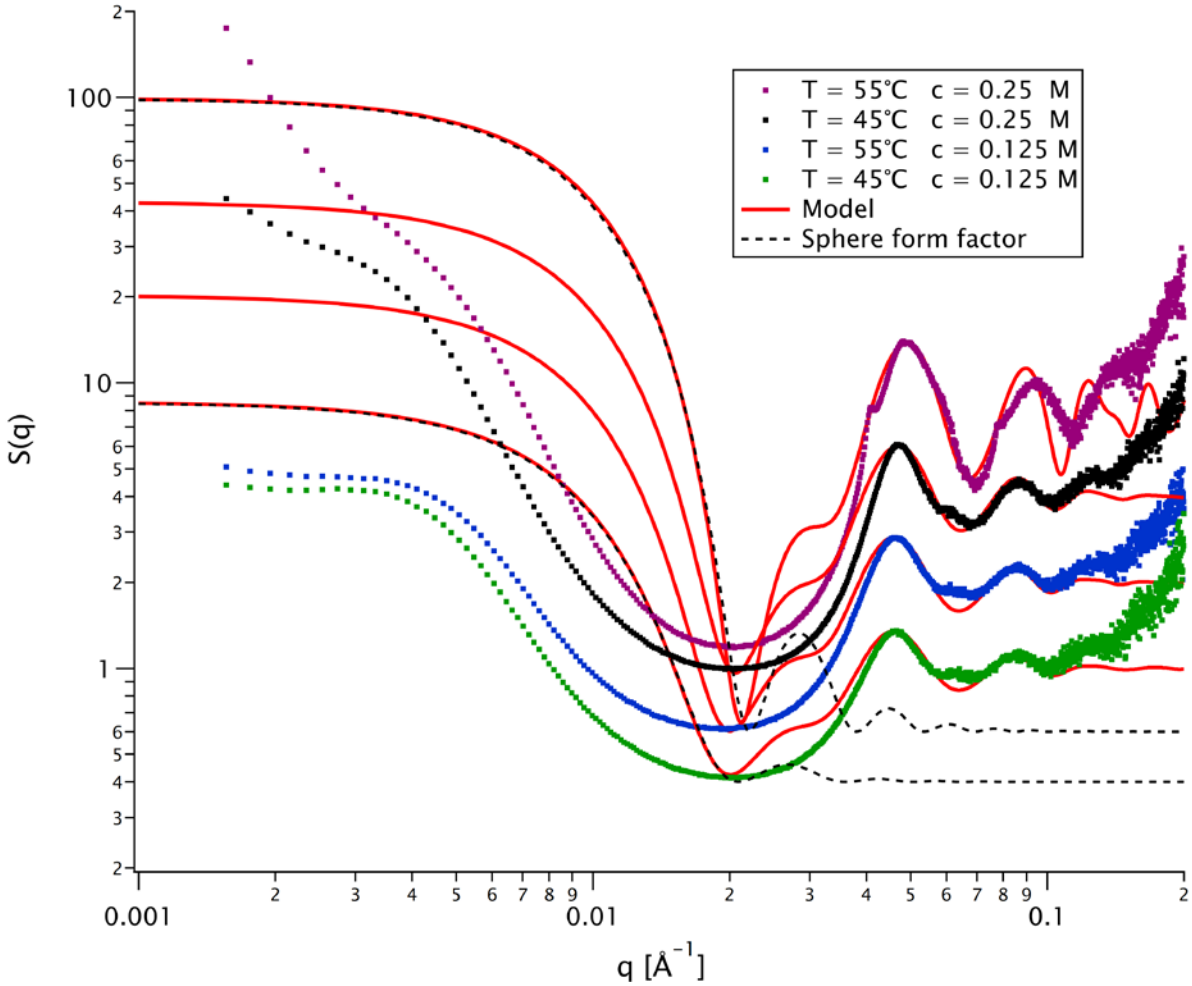

***Figure S7**: Experimental S(q) (colored dots) and model (solid red lines) from Figure 3 in the main text, in log-log representation. The curves are shifted upwards by successive factors of 2. The form factor of a homogeneous sphere that best describes the small q range of the model is shown as dashed line for two curves.*

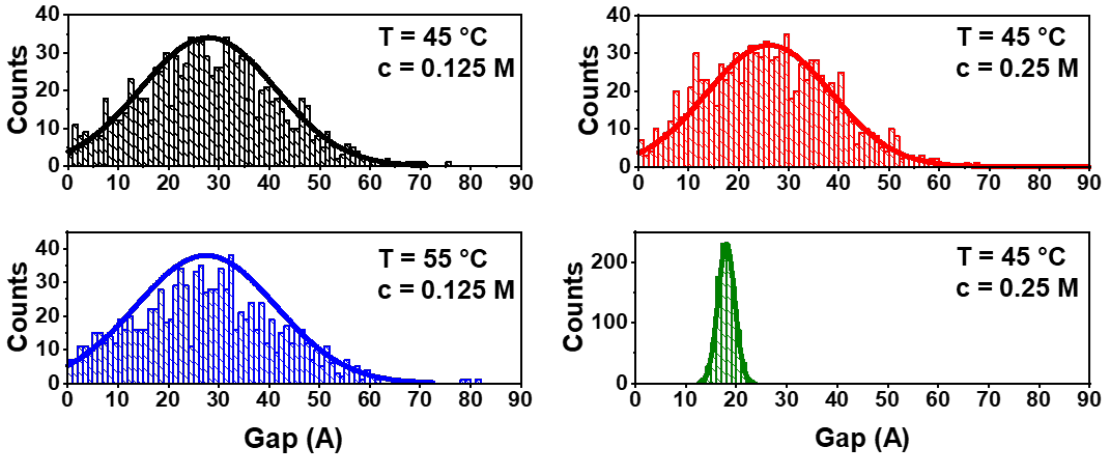

Mean	Standard Deviation	Skewness	Kurtosis	Minimum	Median	Maximum
27.9	13.3	0.2	-0.2	0.4	27.4	75.3
26.0	12.4	0.2	-0.4	0.1	25.6	67.1
27.5	13.8	0.3	-0.1	0.1	27.4	81.3
18.0	1.7	0.0	-0.2	13.4	18.0	23.9

***Figure S8**: Distribution of interparticle distances at different temperatures and ion concentrations.*

Colloidal interaction calculation

The colloidal pair interaction potential calculation was performed by summing up dispersion, electric double layer, and steric interaction terms:

$$U(D) = U_{disp}(D) + U_{EDL}(D) + U_{st}(D)$$

During calculations the SAXS derived particle size (a=7.1 nm) was used. Given the characteristic steep increase of the steric repulsion, for the effective PEG chain length the average surface separation distances obtained from SAXS (See Table 1 in the main text) have been divided by a factor of 2 and used as input in the calculation on the steric repulsion. For the as-prepared nanoparticles PEGylated particles zeta-potential of -9 mV was used. The dispersion interaction was calculated in the usual form of:

$$U_{Disp} = -\frac{A_{HAM}}{3}\left[\frac{a^2}{D(4a+D)} + \frac{a^2}{(2a+D)^2} + \frac{1}{2}ln\left(1 - \frac{4a^2}{(2a+D)^2}\right)\right]$$

where a is the particle radius, D the surface-to-surface separation and AHAM the Hamaker coefficient (2.5×10−19 J).[1] The electric double layer interaction was calculated based on effective scaled surface potentials,[2] steric interaction has been implemented as reported earlier.[3] It has to be noted though, that at the investigated salt concentrations the repulsion contribution of electric double layer interaction to the total interaction is limited and the net pair-interaction is dominated by the interplay between the attractive dispersion and repulsive steric interaction. This is clear if one compares the Debye length (κ^{-1}) with the native PEG brush thickness. The former can be calculated based on the concentration of used 1:2 electrolyte (Figure S7, right) and shows that at 0.125 and 0.25 M concentration the Debye length is well below 1 nm.[4] While the plotted values are calculated at 25°C, at the highest temperature investigated (55°C) these increase only marginally (from 0.50 to 0.52 nm at 0.125M and from 0.35 to 0.37 nm at 0.25 M, respectively). In comparison, the native PEG brush thickness on the as-prepared nanoparticles extends much further; around 1.85 ± 0.1 nm, as derived earlier from dynamic light scattering experiments for the same system.[3] The brush type PEG-graft on the Au spheres due the high grafting density (above 4/nm^2) was shown in an earlier literature report based on DLS and TGA measurements.[5]

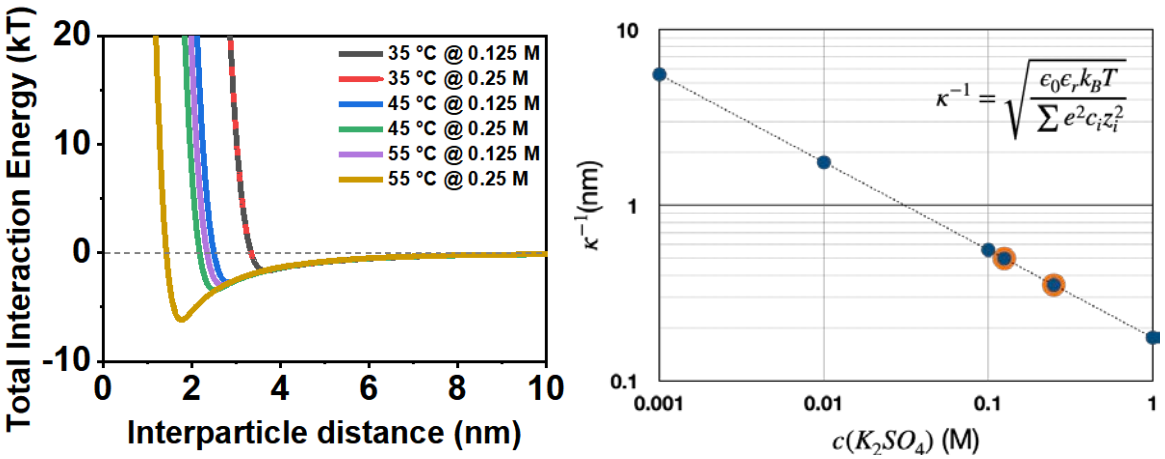

***Figure S9**: Calculated total interaction energy at different temperatures and salt concentrations (left). Log-log plot of the calculated Debye length (κ^{-1}) at 25 °C as a function of the 1:2 electrolyte*

concentration (right). The two orange-colored points mark the concentration values used during the experiments (0.125 and 0.25M, respectively).

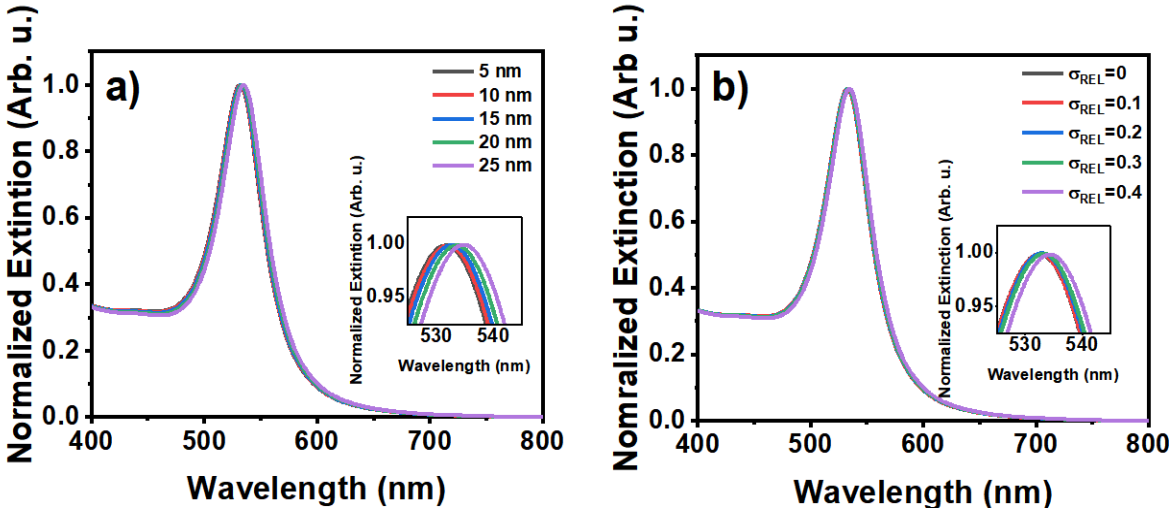

***Figure S10**: Calculated extinction spectra of spherical gold nanoparticles with different size from 5 nm to 25 nm (a). Simulated mean extinction spectra of particles with different standard deviation (b). The insets show the zoomed graph of the extinction spectra close to the resonance peak.*

References

1 S. Biggs and P. Mulvaney, *The Journal of Chemical Physics*, 1994, **100**, 8501–8505.

2 Y. Zheng, L. Rosa, T. Thai, S. H. Ng, D. E. Gómez, H. Ohshima and U. Bach, *Journal of Materials Chemistry A*, 2015, **3**, 240–249.

3 D. Zámbó, G. Z. Radnóczi and A. Deák, *Langmuir*, 2015, **31**, 2662–2668.

4 J. N. Israelachvili, *Intermolecular and surface forces*, Academic Press, Burlington, MA, 3rd ed., 2011.

5 K. Rahme, L. Chen, R. G. Hobbs, M. A. Morris, C. O'Driscoll and J. D. Holmes, *RSC Advances*, 2013, **3**, 6085.